Strain-driven spin-state transition and superexchange interaction in $LaCoO_3$: *Ab initio* study

Hosung Seo, Agham Posadas, and Alexander A. Demkov*
Department of Physics, University of Texas at Austin, Austin, Texas 78712, USA
(Received 26 January 2012; revised manuscript received 17 June 2012; published 26 July 2012)

Using spin density functional theory with the Hubbard correction, we investigate the magnetic structure of strained $LaCoO_3$. We show that beyond biaxial tensile strain of 2.5%, local magnetic moments originating from the high spin state of Co^{3+} emerge in a low spin Co^{3+} matrix. In contrast, we find that compressive strain is not able to stabilize a magnetic state due to geometric constraints. $LaCoO_3$ accommodates tensile strain via spin-state disproportionation, resulting in an unusual sublattice structure. In tensile-strained $LaCoO_3$, the first nearest-neighbor (n.n.) exchange coupling is ferromagnetic (FM), while the second n.n. interaction is stronger and antiferromagnetic (AFM). This unusual feature of the exchange parameters is qualitatively verified with a model superexchange calculation. Due to the competition between the FM and the AFM couplings in the system, we find that the most probable magnetic structure of tensile-strained $LaCoO_3$ is a canted-spin structure, which may explain the relatively small observed magnetic moment of $0.7\mu_B/Co^{3+}$.

DOI: 10.1103/PhysRevB.86.014430 PACS number(s): 75.30.Wx, 71.15.Mb

I. INTRODUCTION

Artificial heterostructures with functional perovskite oxides as building blocks can be synthesized using advanced thin film deposition techniques.[1] Furthermore, strain engineering in these oxide heterostructures opens routes for creating novel electronic phases.[2–4] An exciting example is the recent demonstration of biaxial tensile strain stabilizing an insulating ferromagnetic (FM) ground state in $LaCoO_3$ (LCO).[5–14] Although LCO is a classic example of a correlated $3d$ transition metal perovskite oxide,[15,16] FM correlation has never been observed for the bulk ground state where the Co^{3+} ions exist in the so-called low spin (LS) state (total spin per Co $S = 0$).[15] Since the first demonstrations by Fuchs *et al*. using films grown by pulsed laser deposition[5] and by our group using molecular beam epitaxy,[10] several intriguing properties of strained LCO have been found experimentally. In addition to transport measurements showing insulating behavior for tensile-strained FM LCO,[7] Fuchs *et al*. showed that both the population of the higher spin states and the magnetization in LCO increase as tensile strain increases.[6] Using x-ray techniques, Merz *et al*. suggested that the magnetic structure of tensile-strained LCO grown on $SrTiO_3$ (STO) is a mixture of Co^{3+} high spin (HS) and Co^{3+} LS states.[13] A recent report by Mehta and Suzuki also suggests that compressive strain by itself cannot produce an FM state in LCO,[12] indicating the existence of an asymmetric orbital–lattice interaction.[4] Magnetization measurements of compressively strained LCO on $LaAlO_3$ (LAO) substrates show only weak to no ferromagnetism.[6,7,12] Most recently, Sterbinsky *et al*. showed that intersite hybridization involving Co and O states in LCO on STO is weaker than that in LCO on LAO by comparing the pre-edge structure of the Co K-edge x-ray absorption spectra.[14] A complete theoretical picture of strained LCO must be able to account for all these experimental observations.

The minimal theoretical model to describe the basic electronic properties of LCO is a $[CoO_6]^{9-}$ octahedron within the ligand field theory.[16] In a cubic crystal field, the localized $3d$ orbitals are split into doubly degenerate e_g (d_{z^2} and $d_{x^2-y^2}$) and triply degenerate t_{2g} (d_{xy}, d_{yz}, and d_{zx}) states separated by the crystal field splitting $10Dq$. Other important energy scales are the on-site Hubbard repulsion U, Hund's exchange coupling J_H, and the hopping matrix between the Co $3d$ and the O $2p$ orbitals t. Because all competing interactions are of the same order, Co^{3+} can access different spin states: LS ($t_{2g}^6 e_g^0$, $S = 0$), intermediate spin (IS, $t_{2g}^5 e_g^1$, $S = 1$), or HS ($t_{2g}^4 e_g^2$, $S = 2$). The ground state is insulating and nonmagnetic (NM) with Co^{3+} in the LS state. LCO undergoes a crossover to a paramagnetic insulating phase $\sim$100 K and a metal–insulator transition above 500 K.[17] However, the spin structure at different temperatures has been highly debated. For example, the LS-HS,[17,18] LS-IS,[19,20] and LS-HS/LS crossover scenarios have been discussed in the literature.[21–25]

While a substantial body of experimental results for strained LCO has been reported, there is a clear lack of theoretical understanding taking into account all experimental observations.[10,26–28] Using density functional theory (DFT), Gupta and Mahadevan claimed that tensile strain is able to stabilize an FM ground state in LCO,[26] while Rondinelli and Spaldin suggested that strain by itself cannot produce an FM state.[27] However, Coulomb correlation effects for the localized $3d$ orbitals in LCO were not considered in Ref. 26, and proper structural optimization has not been performed in Ref. 27. In our previous work, using local spin density approximation combined with the Hubbard U correction (LSDA + U), we showed that an FM state based on a homogenous IS state ($S = 1$) can be stabilized above 3.8% tensile strain.[10] The FM IS state is, however, inconsistent with two experimentally determined properties of strained LCO: the IS state is half-metallic, while an experiment shows that strained LCO is insulating,[7] and a rather high critical strain of 3.8% is required, which is somewhat higher than that in experiment ($\sim$2%).[5–10] Most recently, using LSDA + U, Hsu *et al*. showed that a HS/LS mixed state has a lower energy than that of the IS state in tensile-strained LCO on STO.[28] They also suggested that the proposed HS/LS state is FM coupled via superexchange interaction by considering the nearest-neighbor (n.n.) interaction.

In this article, using first-principles calculations, we expand our previous theoretical work on strained LCO[10] by considering homogeneous IS states and inhomogeneous HS/LS mixed

states as functions of biaxial strain from −4% to 4%. We show that beyond a tensile strain of 2.5%, LCO undergoes a spin-state transition from LS to mixed HS/LS states,[13] and we explain why the higher concentration of HS Co^{3+} is preferred in tensile-strained LCO.[6] This feature of our theory is due to reduced mixing between the Co $3d$ and the O $2p$ states in the HS CoO_6 units, leading to softer HS Co-O bonds compared to those of the LS CoO_6 units.[14] The HS/LS state has an energy gap of 0.5 eV, which is consistent with tensile-strained FM LCO being insulating.[7] However, we show that no magnetic state is stable under compressive strain.[4,6,7,12]

To understand the FM ordering in tensile-strained LCO found in the experiment, we calculate the first and second n.n. exchange parameters in the 1:1 HS/LS state.[29,30] The qualitative feature of the exchange parameters is further verified within a model superexchange calculation. We show that the first n.n. coupling is FM. However, the second n.n. coupling is strongly antiferromagnetic (AFM). As a result, we find that the most stable collinear magnetic structure of the HS/LS state is not an FM structure, but an AFM one with a $\uparrow\uparrow\downarrow\downarrow$ order in the c direction. However, the energy difference between the FM and the AFM solutions is very small ($\sim 2 \sim 3$ meV/Co^{3+}). Furthermore, several noncollinear magnetic structures are degenerate in energy with the collinear AFM solution. Moreover, a small magnetic field is typically applied in experiment, so we argue that a canted magnetic structure with a net magnetization could be stabilized.

The rest of the paper is organized as follows: In Sec. II, we explain the computational details; in Sec. III, we examine the stability of various magnetic configurations under epitaxial strain; in Sec. IV, to explore the mechanism of strain-induced spin-state transition in LCO, we discuss the electronic and structural response of LCO to applied strain, depending on its magnetic state; in Sec. V, we calculate the exchange parameters in the 1:1 HS/LS configuration and describe the superexchange paths using an effective e_g model; in Sec. VI, we discuss a possible spin-canted magnetic structure of tensile-strained LCO; and in Sec. VII, we summarize our main results.

II. COMPUTATIONAL DETAILS

The calculations are done using DFT as implemented in the Vienna *ab initio* simulation package code,[31] along with projector-augmented wave pseudopotentials to describe La, Co, and O[32] and a cutoff energy of 600 eV. The valence configurations for the elements are $5s^2 5p^6 5d^1 6s^2$ for La, $3d^7 4s^2$ for Co, and $2s^2 2p^4$ for O. Each self-consistent electronic calculation is converged to 10^{-6} eV/cell, and the tolerance factor for the ionic relaxation is set to 0.01 eV/Å. We employ LSDA + U in the rotationally invariant formalism[33,34] to describe the static electronic correlation effect of $3d$ electrons of the Co^{3+} ion. For the exchange–correlation energy part of the LDA functional, we use the Perdew-Zunger parameterization of the Ceperly-Alder data.[35] For the Hubbard U correction, we use the Dudarev formalism to describe the local moment formation in strained LCO applying U_{eff} ($=U-J$) of 3.8 eV on the Co $3d$ orbitals. In addition, we check that the original Liechtenstein's rotationally invariant functional, with $U = 5.27$ eV and $J = 1.47$ eV,[36]

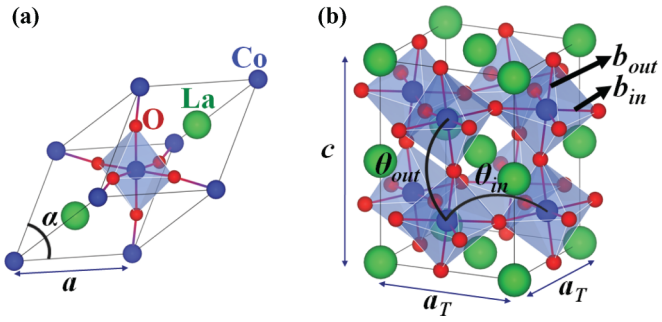

FIG. 1. (Color online) (a) Rhombohedral unit cell of LCO with the large sphere representing La, the medium-sized sphere representing Co, and the small sphere representing O. (b) $\sqrt{2} \times \sqrt{2} \times 2$ tetragonal supercell of LCO. b_{in} and b_{out} stand, respectively, for the in-plane and the out-of-plane Co-O bond length. θ_{in} and θ_{out} stand, respectively, for the in-plane and the out-of-plane Co-O-Co bond angle.

gives qualitatively the same electronic structure for the HS/LS mixed states. The rationale for the U value is based on the following: (1) It is consistent with the existing photoemission and cluster calculation data ($U \approx 5 \sim 5.5$ eV);[37–39] (2) it produces an NM semiconducting ground state with an energy gap of 0.7 eV, in good agreement with the experimental value of $0.6 \sim 0.9$ eV;[37,40] and (3) the theoretical structure is in good agreement with experiment.[41] The ground state structure of LCO is shown in Fig. 1(a). It is described with space group $R\bar{3}c$ with a distorted corner-sharing CoO_6 octahedral network ($a^-a^-a^-$ in the Glazer tilt system[42,43]). We compare the calculated structural parameters for bulk LCO with experiment in Table I.

Motivated by the coherent cube-on-cube epitaxy of LCO with thickness of ∼40 nm on STO,[10,11] we consider pure strain effects by performing "strained-bulk" calculations using supercells. To examine the stability of various magnetic states in tensile-strained LCO, we use three cell types: $\sqrt{2} \times \sqrt{2} \times 2$, $\sqrt{2} \times \sqrt{2} \times 4$, and $2 \times 2 \times 2$ with respect to a five-atom pseudo-cubic cell, for which $6 \times 6 \times 4$, $6 \times 6 \times 2$, and $4 \times 4 \times 4$ Monkhorst-Pack k-point grids, respectively, are used for the Brillouin zone integration.[44] To describe the effect of strain on the electronic and magnetic properties of LCO, we use the $\sqrt{2} \times \sqrt{2} \times 2$ cell shown in Fig. 1(b). We vary the in-plane lattice parameter a_T biaxially and optimize the c axis lattice constant and all internal degrees of freedom without any structural constraints. Strain is defined as $(a_T - a_{\text{pc}})/(a_{\text{pc}})$, where a_{pc} is the pseudo-cubic lattice parameter of NM LCO, which is calculated to be 3.74 Å. We consider biaxial strain levels in the range from −4% to 4%. The optimized c and

TABLE I. Ground state structure ($R\bar{3}c$) of NM insulating LCO.

	a (Å)	α (°)	x	Co-O length (Å)	Co-O-Co angle (°)
Theory (this work)	5.249	61.13	0.5528	1.893	162.87
Experiment[a] ($T = 5$ K)	5.345	61.01	0.5527	1.925	162.93

[a]Reference 20.

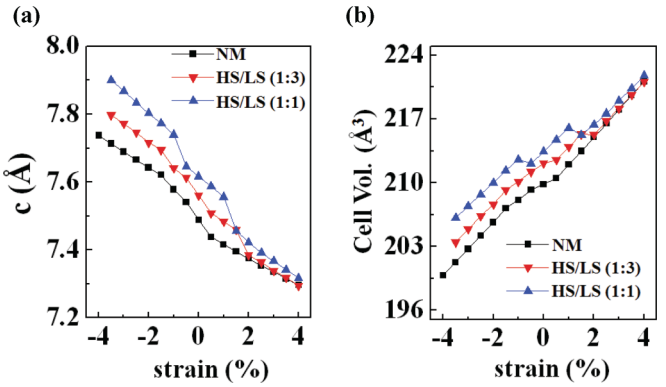

FIG. 2. (Color online) (a) Optimized c lattice constant and (b) cell volume of LCO with different magnetic states. NM means NM LCO. HS/LS (1:3) or (1:1) mean FM LCO with a HS/LS mixed spin state with the ratio of 1:3 or 1:1, respectively.

cell volume of LCO with different magnetic states are shown in Fig. 2. The overall trend shown in Fig. 2 is that under tensile strain, LCO tends to shrink in the c direction due to the Poisson effect while the cell volume increases as a function of strain; under compressive strain, LCO tends to expand in the c direction while the cell volume decreases. Finally, to calculate the exchange coupling constants, we use $2 \times 2 \times 4$ and $4 \times 2 \times 2$ supercells, for which $4 \times 4 \times 2$ and $2 \times 4 \times 4$ k-point meshes are used, respectively.

III. STRAIN-INDUCED SPIN-STATE TRANSITION IN LCO

We start our investigation by searching for the most stable magnetic solution in LCO on STO at low temperature (theoretical strain = 3.5%). We use $\sqrt{2} \times \sqrt{2} \times 2$, $\sqrt{2} \times \sqrt{2} \times 4$, and $2 \times 2 \times 2$ cells for which the c axis lattice constant and the internal structure are optimized for each magnetic configuration. We first test homogeneous magnetic configurations with all Co^{3+} in either the IS or the HS state. For the homogeneous HS state, only an AFM-aligned solution (G-type) is stabilized. This is consistent with the Goodenough-Kanamori-Anderson rule[45] stating that the indirect superexchange between half-filled orbitals, mediated by O $2p$ with an angle close to 180°, is AFM. At 3.5% tensile strain, however, the homogeneous IS state is still 15 meV/formula unit higher in energy than the NM state, with the homogeneous HS state 250 meV/formula unit higher in energy than the IS state. In addition, the homogeneous IS state is half-metallic, while experimentally, strained LCO shows an insulating behavior.[7] Therefore, we conclude that the homogeneous magnetic configurations are unlikely to be the magnetic structure of tensile-strained LCO.

We next consider mixed magnetic configurations where HS Co^{3+} ions are embedded in a LS Co^{3+} matrix. We compare the total energy of 22 HS/LS configurations, where various geometric arrangements of HS Co^{3+} ions are considered. We have also compared various FM- and AFM-ordered states. However, we find that the dominant energy scale determining the stability of the system is provided by the concentration and arrangement of the HS Co^{3+} ions with an energy scale of 100 meV/cell, as shown in Fig. 3(a). Therefore, our strategy is to first consider FM-ordered HS/LS states to study the overall stability and behavior of the HS/LS configurations

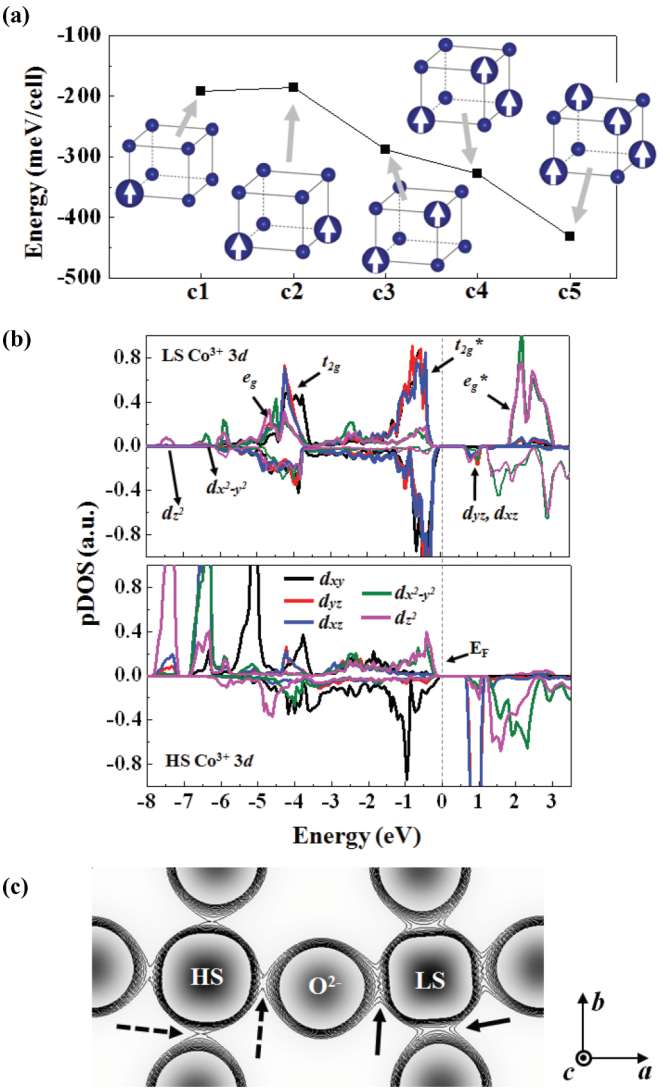

FIG. 3. (Color online) (a) Energy of LCO with HS/LS mixed spin states per $2 \times 2 \times 2$ cell (8 formula units) under a tensile strain of 3.5%. Energy of NM LCO is set to 0 eV. Insets are schematic pictures of the geometrical arrangement of HS Co^{3+} ions for each HS/LS configuration (c1–c5). Dark spheres indicate Co^{3+} sites, with La and O sites omitted for clarity. White arrows in the large spheres represent spins at the HS Co^{3+} sites. (b) Projected density of states for $3d$ orbitals in the 1:1 HS/LS mixed state [c5 in Fig. 3(a)] at the LS Co^{3+} site (upper panel) and the out-of-plane HS Co^{3+} site (lower panel). The Fermi energy (dashed vertical line) is set to 0 eV. The positive and negative densities of states are for spin up and spin down, respectively. (c) Cross-sectional valence charge distribution of the 1:1 HS/LS mixed state at the CoO_2 plane with contours overlaid. The contours are drawn for the charge density from 0.5 to 1.0 eÅ^{-3} using a step interval of 0.04 eÅ^{-3} to contrast the charge accumulations at the HS Co-O bonds (dotted arrows) with the LS Co-O bonds (solid arrows).

under epitaxial strain. In Sec. V, we explore the exchange interaction in the HS/LS state with the most stable geometrical configuration under tensile strain.

The first important finding is that when LCO forms HS Co^{3+} ions, it is energetically favorable to separate them by LS Co^{3+} rather than having them be the first n.n.s. Furthermore, we find

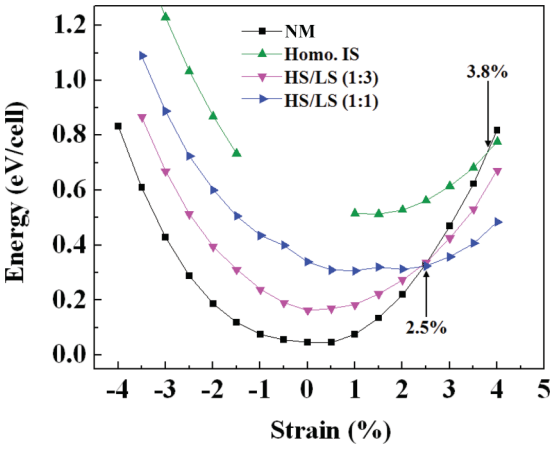

FIG. 4. (Color online) Energy of LCO per $\sqrt{2} \times \sqrt{2} \times 2$ cell (4 formula units) as a function of strain for NM (filled squares), homogeneous (Homo.) IS (up triangles), 1:3 HS/LS (down triangles), and 1:1 HS/LS (right triangles) states.

that tensile-strained LCO becomes more stable as the number of these second n.n. HS pairs increases, as shown in Fig. 3(a). Overall, we find that a 1:1 HS/LS mixed configuration [c5 in Fig. 3(a)] is the most stable magnetic solution for LCO under 3.5% strain. The total energy of this configuration is 54 meV/formula unit below that of NM LCO. In Fig. 3(b), we show the $3d$-projected density of states at the LS and upper HS Co^{3+} sites in the c axis direction for the 1:1 HS/LS state. There is an energy gap of 0.5 eV at the Fermi level defined by the $t_{2g}{}^*$ and $e_g{}^*$ splitting of the LS Co^{3+} sites. For the HS Co^{3+} site, the on-site U and J produce localized states from -8.0 to -5.0 eV in the spin-up channel, and empty d_{xz} and d_{yz} states in the spin-down channel, consistent with the mean field picture of the HS state. The presence of the energy gap in the HS/LS mixed state is consistent with strained LCO being insulating.[7]

To elucidate the effect of epitaxial strain on the magnetic state of LCO, we compare in Fig. 4 the energy as a function of strain for mixed HS/LS configurations, with 25% and 50% concentrations of HS Co^{3+}, the homogeneous IS state (previously considered in Ref. 10), and NM LCO for reference. The HS/LS mixed states are stable when compared to the homogeneous IS state at all strain levels, and above a tensile strain of 2.5%, the HS/LS states become more stable than NM LCO. Under zero strain, there is an energy cost to excite LS Co^{3+} to HS Co^{3+}. Comparing the energy of a dilute HS/LS configuration with a HS Co^{3+} concentration of 12.5% to that of NM LCO, we estimate the energy cost of the excitation to be 62 meV/Co^{3+}. However, as a function of tensile strain, the energy of the mixed HS/LS states (see Fig. 3) increases more slowly than that of NM LCO, inducing a spin-state transition at 2.5%. It is also evident from Fig. 4 that LCO with a higher concentration of HS Co^{3+} is softer against tensile strain[6] and that compressive strain doesn't stabilize a magnetic state.[6,7,12]

IV. ELECTRONIC AND STRUCTURAL RESPONSE OF LCO UNDER EPITAXIAL STRAIN

To shed more light on the mechanism of the strain-induced spin-state transition in LCO, we plot the energy gap in NM LCO as a function of strain in Fig. 5(a). The energy gap in LCO forms between the $t_{2g}{}^*$ and the $e_g{}^*$ bands and is given by $10Dq - [W(e_g{}^*) + W(t_{2g}{}^*)]/2$, where $10Dq$ is the crystal field splitting and the Ws are the bandwidths of corresponding bands. Under epitaxial strain, the local symmetry at the Co^{3+} site is lowered from cubic O_h to tetragonal D_{4h}, and the degeneracy in the $t_{2g}{}^*$ and $e_g{}^*$ manifolds is lifted, as shown in Fig. 5(b). Furthermore, the change in the Co-O bond length and the Co-O-Co bond angle modifies the bandwidths.[46] In Fig. 5(a), we see that the energy gap becomes less than 58 meV above a strain level of 2.5%, thus allowing the spin-state transition.[22] The band gap also narrows for compressively strained LCO, but this does not result in a magnetic solution, as shown in Fig. 4. Our result suggests that the standard picture in terms of the competition between the crystal field splitting and the Hund rule coupling is not sufficient to consistently describe magnetism in strained LCO. Instead, an important structural transition in LCO under tensile strain accompanies the spin-state transition.

When biaxially strained, LCO responds in the out-of-plane c direction due to the Poisson effect[6,10] (see Fig. 2). Because the LS CoO_6 unit is rigid due to covalency of the Co-O bond (bond stretching costs a large amount of energy), strain is mainly accommodated by tilting and rotating CoO_6 octahedra.[47] Microscopically, this is achieved by changes in the Co-O-Co

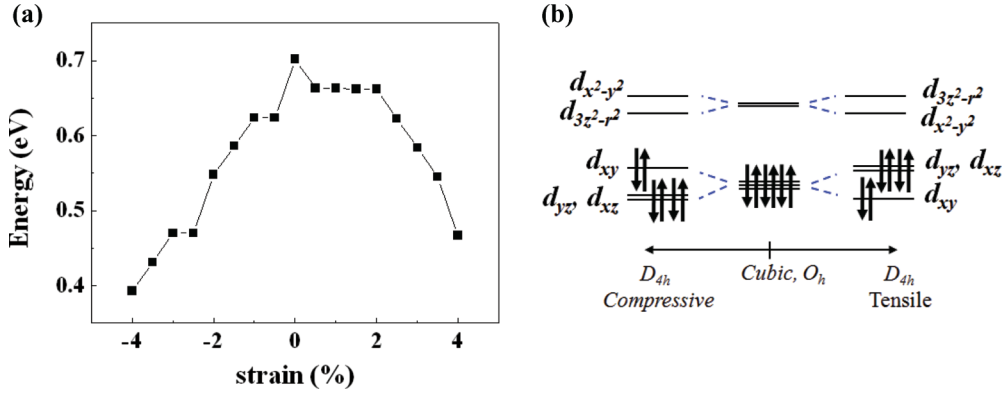

FIG. 5. (Color online) (a) Energy gap between the $t_{2g}{}^*$ and the $e_g{}^*$ bands of NM LCO as a function of strain. (b) Energy level splitting of LS Co^{3+} under compressive or tensile strain.

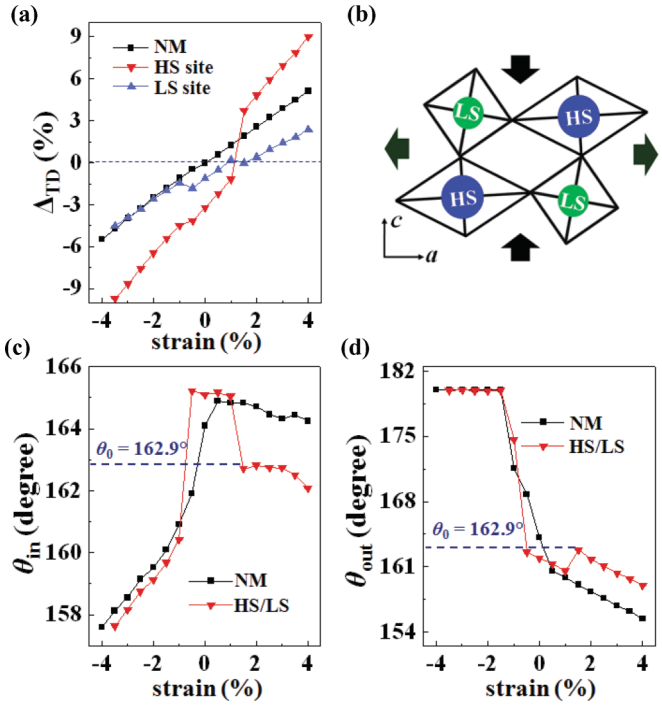

FIG. 6. (Color online) (a) Local tetragonality ($\Delta_{TD} = 2 \times (b_{in} - b_{out})/|b_{in} + b_{out}|$) as a function of strain for CoO_6 octahedra in NM LCO (squares), for HS Co^{3+} sites (down triangles), and LS Co^{3+} sites (up triangles) in 1:1 HS/LS FM LCO. (b) Schematic of octahedral distortion in 1:1 HS/LS FM LCO above 1.5% strain. Lateral arrows stand for the epitaxial constraint in the ab plane imposed by biaxial tensile strain, while vertical arrows stand for the contraction of LCO in the c direction due to the Poisson effect. (c) In-plane and (d) out-of-plane Co-O-Co angles as a function of strain for NM LCO (squares) and 1:1 HS/LS FM LCO (triangles). θ_0 is the theoretical Co-O-Co angle in the LCO bulk.

angles [θ_{in} and θ_{out} in Fig. 1(a)], accompanied by slight changes in the Co-O bond length [b_{in} and b_{out} in Fig. 1(a)] or local tetragonality ($\Delta_{TD} = 2 \times (b_{in} - b_{out})/|b_{in} + b_{out}|$). As shown in Fig. 6(a), in NM LCO, local tetragonality increases almost linearly as tensile or compressive strain is applied. In a simple model, the energy curve for NM LCO in Fig. 4 could be thought of as $\frac{1}{2}k\Delta_{TD}{}^2$, where k is a spring constant determined by the covalent mixing between the Co $3d$ and the O $2p$ states. Therefore, to minimize the bond stretching or Δ_{TD} under tensile strain, the octahedral rotation is largely suppressed (θ_{in} greater than the bulk value) while the tilting is enhanced (θ_{out} smaller than the bulk value), as shown in Figs. 6(c) and 6(d). The opposite is true for compressive strain: θ_{in} becomes smaller than the bulk value, in conjunction with the disappearance of the tilting mode ($\theta_{out} = 180°$).

Interestingly, we find that strained 1:1 HS/LS LCO undergoes an unusual structural transition above 1.5% tensile strain. It manifests as a substantial increase in Δ_{TD} of the HS CoO_6 clusters, as shown in Figs. 6(a) and 6(b). However, Δ_{TD} of the LS clusters in 1:1 HS/LS LCO drops by more than a factor of two compared to NM LCO. This suggests that above 1.5%, tensile strain is accommodated mainly by the HS CoO_6 units through bond length changes, allowing the LS octahedra to be less distorted and thus relieving their elastic energy. This is possible because HS Co^{3+} has a softer Co-O bond under stretch.[48–50] As a result, both bond angles θ_{in} and θ_{out} almost recover their bulk values, because octahedral rotation and tilting are no longer needed for strain accommodation [Figs. 6(c) and 6(d)].

One way to rationalize this effect is to assume that at the spin-state transition under tensile strain, the spring constant between HS Co^{3+} and O becomes k', which is significantly less than k of LS CoO_6 units. This is evident from the electronic structure shown in Fig. 3(b). The strong on-site interactions U and J produce localized orbitals for the HS configuration while sacrificing the hybridization between Co $3d$ and O $2p$. In Fig. 3(c), we show the valence charge distribution in the CoO_2 plane for the 1:1 HS/LS mixed state. Less charge is accumulated along the HS Co-O bonds due to reduced hybridization when compared to that of the LS Co-O bonds.[14] Therefore, although replacing LS Co^{3+} ions with HS ones costs energy (~62 meV/Co^{3+}), the relative softness of HS CoO_6 clusters pays off beyond 2.5% strain. On the contrary, this type of structural transition does not occur under compressive strain, as shown in Fig. 4(a). If it were to occur, the HS CoO_6 units would further contract in the ab plane, which is incompatible with the known tendency of HS Co^{3+} to occupy a larger local volume.[20,51]

V. SUPEREXCHANGE INTERACTION IN THE 1:1 HS/LS MIXED STATE

The magnetic moments in the mixed 1:1 HS/LS configuration of 3.5% tensile-strained LCO are well localized at the HS Co^{3+} sites. Therefore, to map the exchange coupling between the local moments, we use an effective Heisenberg Hamiltonian for the exchange energy of the system:[29,30]

$$H = -\sum_{i \neq j} J^{ij} \vec{e}_i \cdot \vec{e}_j, \quad (1)$$

where $\vec{e}_i$ and $\vec{e}_j$ are the local moments at site i and j, respectively, and J^{ij} are the exchange parameters. We consider five collinear magnetic configurations, as shown in Fig. 7, to calculate the parameters for the first (coordination number = 12) and the second (coordination number = 6) n.n. interactions. The in-plane exchange constant J is different from the out-of-plane J because of the tetragonal distortion in strained LCO on STO. This yields four coupling constants: $J_{1,in}$, $J_{1,out}$, $J_{2,in}$, and $J_{2,out}$. To calculate $J_{1,in}$ and $J_{1,out}$, we use the 2 × 2 × 2 cell [Fig. 7(a)], while we double the cell along the a axis (the c axis) to calculate $J_{2,in}$ ($J_{2,out}$) [Fig. 7(b)]. Both J_1 coupling constants and J_2 coupling constants are important to consider on the same footing, because two adjacent HS Co^{3+} pairs interact via a superexchange mechanism,[53,54] involving virtual hopping of e_g electrons and t_{2g} holes from HS Co^{3+} sites to the n.n. LS Co^{3+} site. As shown in Fig. 7, both the first and the second n.n. HS Co^{3+} pairs are separated by one LS Co^{3+} ion but with different angles: 90° for the first and 180° for the second n.n HS Co^{3+} pair. This means that the interaction strength is of the same order of magnitude in both cases. In Table II, we list the exchange energies of the magnetic configurations in Fig. 7, along with the calculated exchange parameters. We find that the first n.n. couplings $J_{1,in}$ and $J_{1,out}$ are FM and 2.5 and

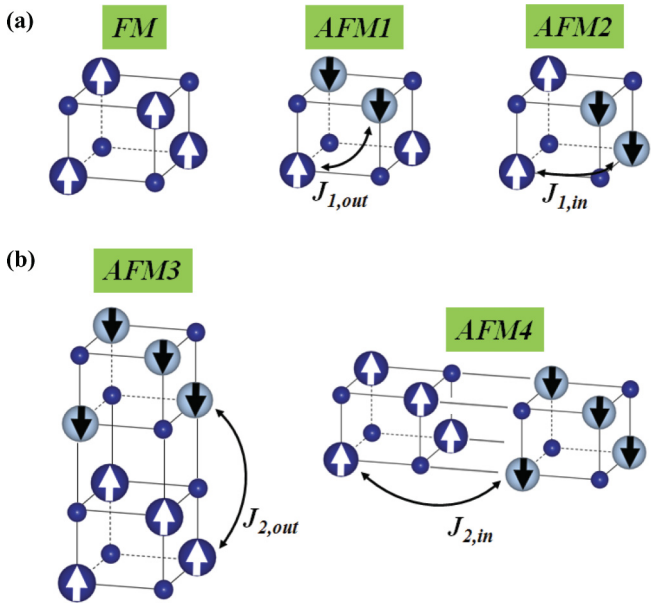

FIG. 7. (Color online) Schematic pictures of collinear magnetic structures of HS/LS mixed states. (a) To calculate the first n.n. coupling parameters ($J_{1,\mathrm{out}}$ and $J_{1,\mathrm{in}}$), the $2 \times 2 \times 2$ supercell is used. (b) The $2 \times 2 \times 4$ (left) or $4 \times 2 \times 2$ (right) supercell is used for the second n.n. coupling parameters ($J_{2,\mathrm{out}}$ and $J_{2,\mathrm{in}}$). Subscripts *out* and *in* for the coupling parameters stand for out-of-plane and in-plane, respectively. Dark spheres indicate Co^{3+} sites, with La and O sites omitted for clarity. White and black arrows in the large spheres represent spins at the HS Co^{3+} sites.

2.7 meV/pair, respectively.[55] However, the second n.n. couplings are strongly AFM, and $|J_{2,\mathrm{out}}|$ is larger than the $|J_1|$ couplings by more than a factor of two.

To better understand the qualitative features of the exchange parameters, we consider an effective e_g model, where the relatively small hopping matrix elements between t_{2g} electrons are not included.[56] In Fig. 8(a), we show the configuration of the 1:1 HS/LS state in the ac plane. The key difference between the first and the second n.n. interactions originates from the hopping matrices. The first n.n. coupling involves both the out-of-plane and the in-plane hopping matrices, which are described by t_c and t_a, respectively. Considering the orbital symmetry, t_c and t_a can be written as

$$t_c = t \begin{pmatrix} 1 & 0 \\ 0 & 0 \end{pmatrix} \text{ and } \quad t_a = \frac{t'}{4} \begin{pmatrix} 1 & -\sqrt{3} \\ -\sqrt{3} & 3 \end{pmatrix}, \text{ respectively,} \tag{2}$$

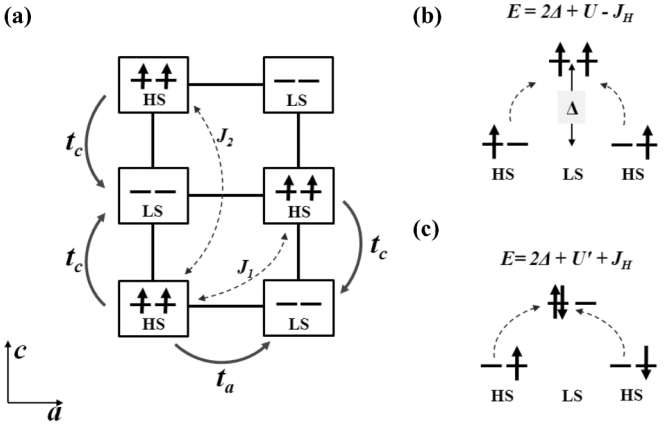

FIG. 8. (a) Schematic of the superexchange paths for the first (J_1) and second (J_2) n.n. couplings of the 1:1: HS/LS mixed state in the ac plane. Only the e_g levels ($|d_{3z^2-r^2}\rangle, |d_{x^2-y^2}\rangle$) are shown. Diagrams illustrating the (b) FM and (c) AFM superexchange interactions for the first and the second n.n. couplings in the 1:1 HS/LS state, respectively. See the main text for the model description.

where we use $\{|d_{3z^2-r^2}\rangle, |d_{x^2-y^2}\rangle\}$ as a basis and $t(t')$ is the effective d-d hopping constant.[56] For the out-of-plane hopping matrix t_c, we only consider the dominant hopping t between $|d_{3z^2-r^2}\rangle$ states for simplicity. Once we fix the hopping matrix along the c axis, the in-plane hopping matrix t_a can be obtained by a coordinate transformation. However, the in-plane hopping parameter t' should be smaller than the out-of-plane t due to the tetragonal distortion in tensile-strained LCO. Using the full e_g bandwidth W of ~4.0 eV in bulk LCO, we estimate the effective d-d hopping for unstrained LCO to be ~0.7 eV ($\sim W/6$).[56] For 3.5% tensile-strained LCO, we showed that the bond angles are close to the bulk values; therefore, the change in the hopping constant under tensile strain mainly arises from the bond length changes. Using our structural data along with Harrison's formula ($t_{dd} \sim 1/d^5$, where d is the interatomic distance),[52] we calculate $t \approx 0.8$ eV and $t' \approx 0.6$ eV.

Let us consider the superexchange path for the first n.n. HS-LS-HS cluster. Table III shows the relevant states for the superexchange interaction in terms of the e_g occupancy at the HS or LS sites. State S1 is the insulating FM- or AFM-ordered ground state of the 1:1 HS/LS state in the absence of hopping. States S2–S4 are virtual excited states that can be reached by one electron hopping from S1. For S2 and S3, we introduce the energy cost Δ for transferring one electron from the HS site to the LS site. In principle, Δ can be determined self-consistently, but we treat it as an empirical parameter in this qualitative

TABLE II. Exchange energy gain for several magnetic configurations,[a] and exchange parameters of the 1:1 HS/LS state of 3.5% tensile-strained LCO.

Configuration[a]	Energy (meV/cell)	Exchange parameter	Strength (meV/pair)
FM	$-8J_{1,\mathrm{in}} - 16J_{1,\mathrm{out}} - 8J_{2,\mathrm{in}} - 4J_{2,\mathrm{out}}$	$J_{1,\mathrm{out}}$	2.7
AFM1	$-8J_{1,\mathrm{in}} + 16J_{1,\mathrm{out}} - 8J_{2,\mathrm{in}} - 4J_{2,\mathrm{out}}$	$J_{1,\mathrm{in}}$	2.5
AFM2	$8J_{1,\mathrm{in}} - 8J_{2,\mathrm{in}} - 4J_{2,\mathrm{out}}$	$J_{2,\mathrm{out}}$	−7.7
AFM3	$-16J_{1,\mathrm{in}} - 16J_{2,\mathrm{in}} + 8J_{2,\mathrm{out}}$	$J_{2,\mathrm{in}}$	−3.3
AFM4	$-16J_{1,\mathrm{out}} - 8J_{2,\mathrm{out}}$		

[a]The collinear magnetic configurations are shown in Fig. 7.

calculation. The most important state for the superexchange interaction is S4, whose energy is determined by the on-site repulsion U and Hund's coupling J_H. For instance, state S4 which is derived from FM-ordered S1 is shown in Fig. 8(b). Considering the hopping matrices t_a and t_c, we construct the Hamiltonian for the FM- and AFM-ordered states as follows:

$$H_{\uparrow\uparrow(\uparrow\downarrow)} = \begin{pmatrix} 0 & t & t'/4 & -\sqrt{3}t'/4 & -\sqrt{3}t'/4 & 3t'/4 & 0 & 0 \\ t & \Delta & 0 & 0 & 0 & 0 & -\sqrt{3}t'/4 & 3t'/4 \\ t'/4 & 0 & \Delta & 0 & 0 & 0 & 0 & 0 \\ -\sqrt{3}t'/4 & 0 & 0 & \Delta & 0 & 0 & t & 0 \\ -\sqrt{3}t'/4 & 0 & 0 & 0 & \Delta & 0 & 0 & 0 \\ 3t'/4 & 0 & 0 & 0 & 0 & \Delta & 0 & t \\ 0 & -\sqrt{3}t'/4 & 0 & t & 0 & 0 & 2\Delta + U - (+)J_H & 0 \\ 0 & 3t'/4 & 0 & 0 & 0 & t & 0 & 2\Delta + U - (+)J_H \end{pmatrix}, \quad (3)$$

where we use $t \approx 0.8$ eV, $t' \approx 0.6$ eV, $U \approx 5.0$ eV, $J_H \approx 1.5$ eV, and $\Delta \approx 2$ eV. The exchange parameter $J_{1,\text{out}}$ is then calculated as

$$-2J_{1,\text{out}} = E(\text{FM}) - E(\text{AFM}), \quad (4)$$

where E(FM/AFM) is the energy gain for the FM/AFM-ordered state due to superexchange.

However, the superexchange interaction of the second n.n. HS-LS-HS cluster in the ac plane only involves the hopping matrix t_c [Fig. 8(a)]. Therefore, the Hamiltonian for the FM-ordered state only involves configurations S1–S3 in Table III, while S4 can contribute to the exchange energy gain for the AFM-ordered state [Fig. 8(b)]. The Hamiltonian matrices are written as

$$H_{\uparrow\uparrow} = \begin{pmatrix} 0 & t & t \\ t & \Delta & 0 \\ t & 0 & \Delta \end{pmatrix} \quad (5)$$

and

$$H_{\uparrow\downarrow} = \begin{pmatrix} 0 & t & t & 0 \\ t & \Delta & 0 & t \\ t & 0 & \Delta & t \\ 0 & t & t & 2\Delta + U' + J_H \end{pmatrix}, \quad (6)$$

where U' is the intraorbital repulsion, for which we use $U' = U + 2J_H$.[16] Including the ab plane exchange interactions, we calculate the exchange parameters as 1.9, 1.2, −7.9, and −3.1 eV for $J_{1,\text{out}}$, $J_{1,\text{in}}$, $J_{2,\text{out}}$, and $J_{2,\text{in}}$, respectively. These results are in qualitative agreement with the DFT results shown in Table II. Therefore, we show that the larger second n.n. AFM coupling parameters originate from the difference between the hopping matrices involved for J_1 and J_2.

TABLE III. States distinguished by the e_g occupancy at the HS and LS Co^{3+} sites and their energies.

State	HS Co^{3+}	LS Co^{3+}	HS Co^{3+}	Energy
S1	2	0	2	0
S2	1	1	2	Δ
S3	2	1	1	Δ
S4	1	2	1	$2\Delta + U - J_H(\uparrow\downarrow)$ $2\Delta + U + J_H(\uparrow\downarrow)$

VI. NONCOLLINEAR MAGNETIC STRUCTURE IN TENSILE-STRAINED LCO

To explore the effect of $J_{2,\text{out}}$ in the 1:1 HS/LS configuration of tensile-strained (3.5%) LCO, we perform several calculations based on the unconstrained noncollinear spin density functional formalism.[57] The spin–orbit coupling is ignored. In these calculations, only the relative angles between the local moments determine the exchange energy. The calculations are done using the $\sqrt{2} \times \sqrt{2} \times 4$ cell that has eight independent Co sites. First, we introduce a polar angle θ for half of the local moments, as shown in Fig. 9(a); then, we calculate the energy of the system as a function of the angle. The magnetic structures with angles θ of zero and 180° correspond to the collinear FM and AFM3 configurations in Fig. 7, respectively. As shown in Fig. 9(a), the fully FM-ordered state is unstable in the presence of the strong second n.n. AFM coupling; as a result, we find that the most stable collinear structure is AFM3 (net magnetization = 0). This is also the case for LCO under different tensile strain levels. However, the energy difference between the FM and the AFM3 structures is small (∼2.3 meV/Co^{3+}).

To search for possible low-energy-canted spin structures in tensile-strained LCO, we introduce an additional azimuthal angle φ for the local moment, as shown in Fig. 9(b). Considering a large set of different θ and φ for each local moment, we find multiple solutions that are degenerate with AFM3. One of the lowest-energy-canted spin structures is shown in Fig. 9(b). The spin moments rotate by 90° (for φ) as it goes to the next upper ab plane according to the second n.n.

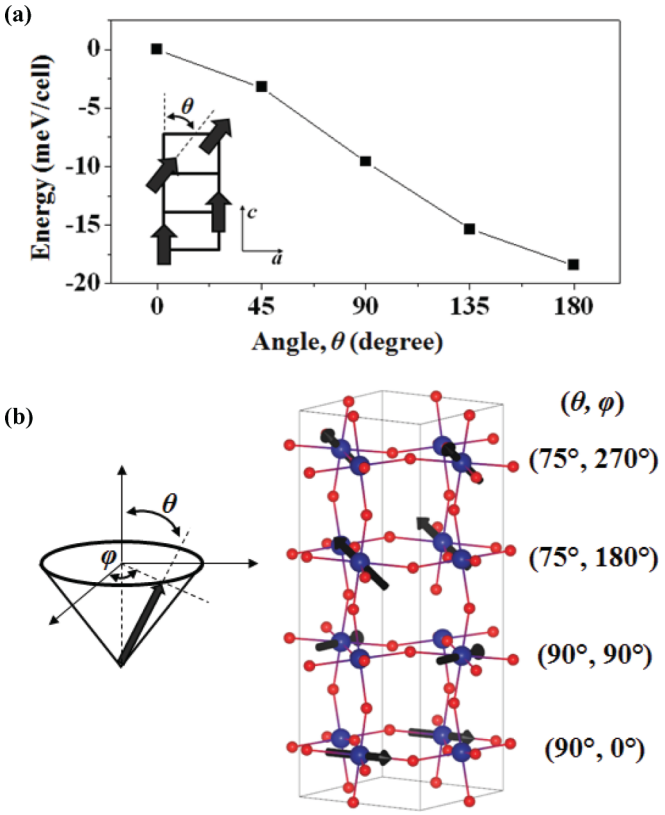

FIG. 9. (Color online) (a) Energy of tensile-strained LCO with the 1:1 HS/LS configuration as a function of canting angle θ. The inset shows a canted spin configuration with angle θ in the ac plane. Black arrows represent the local moments at the HS Co^{3+} sites. The $\sqrt{2} \times \sqrt{2} \times 4$ calculation cell used has 8 formula units. (b) Schematic of a local moment described by polar angle θ and azimuthal angle φ (left). This arrangement is one of the lowest-energy-canted spin structures of tensile-strained LCO (right). La atoms and other small magnetic moments at LS Co^{3+} and O sites are omitted for clarity.

AFM coupling. However, half of the local moments are slightly canted toward the c axis, yielding a small magnetic moment of $\sim 0.26 \mu_B/Co^{3+}$ in the system.[10] Our results suggest that the relatively low magnetic moment of $0.7 \mu_B/Co^{3+}$ in the experiment[10] may be due to the presence of the strong AFM coupling screening the FM ordering in the system. Finally, this particular type of canted structure considered in Fig. 9(b) may not be the lowest-energy structure even in theory, because we are still limited by the size of the cell. Furthermore, in a typical magnetic measurement, a small magnetic field is applied at finite temperature; therefore, another canted FM state may be stabilized.

VII. SUMMARY

We explain the mechanism of strain-induced spin-state transition and examine the exchange interaction in tensile-strained LCO. Considering various high-spin/low-spin configurations, we show that high-spin Co^{3+} ions in LCO prefer to be separated by low-spin Co^{3+} ions. We further demonstrate that above a tensile strain of 2.5%, the ground state of LCO is an insulator with a 1:1 HS/LS mixed state. In contrast, compressive strain is not able to produce a magnetic state. We attribute the stabilization of the HS/LS state to increased compliance of LCO when it has a higher concentration of HS Co^{3+} ions. We examine the exchange parameters in the 1:1 HS/LS state of tensile-strained LCO by considering various collinear magnetic structures. The first n.n. couplings are FM with strengths of 2.5 and 2.7 meV/pair in the in-plane and out-of-plane directions, respectively. However, the second n.n. couplings are strongly AFM with strengths of -3.3 and -7.7 meV/pair in the in-plane and out-of-plane directions, respectively. Due to the strong AFM coupling, we find that the lowest-energy collinear structure is one with an up-up-down-down order in the c direction. However, we show that the competition between the FM and the AFM couplings in the system may lead to a canted (noncollinear) spin structure with a finite net magnetization.

ACKNOWLEDGMENTS

We thank Chungwei Lin for helpful discussions. This work is supported by the National Science Foundation under Grant No. DMR-0548182, the US Department of Energy under Grant No. DE-SC0001878, and Texas Advanced Computing Center.

*demkov@physics.utexas.edu

[1] A. Ohtomo, D. A. Muller, J. L. Grazul, and H. Y. Hwang, Nature **419**, 378 (2002).

[2] J. H. Lee, L. Fang, E. Vlahos, X. Ke, Y. W. Jung, L. F. Kourkoutis, J.-W. Kim, P. J. Ryan, T. Heeg, M. Roeckerath, V. Goian, M. Bernhagen, R. Uecker, P. C. Hammel, K. M. Rabe, S. Kamba, J. Schubert, J. W. Freeland, D. A. Muller, C. J. Fennie, P. Schiffer, V. Gopalan, E. Johnston-Halperin, and D. G. Schlom, Nature **466**, 954 (2010).

[3] R. J. Zeches, M. D. Rossell, J. X. Zhang, A. J. Hatt, Q. He, C.-H. Yang, A. Kumar, C. H. Wang, A. Melville, C. Adamo, G. Sheng, Y.-H. Chu, J. F. Ihlefeld, R. Erni, C. Ederer, V. Gopalan, L. Q. Chen, D. G. Schlom, N. A. Spaldin, L. W. Martin, and R. Ramesh, Science **326**, 977 (2009).

[4] J. Chakhalian, J. M. Rondinelli, J. Liu, B. A. Gray, M. Kareev, E. J. Moon, N. Prasai, J. L. Cohn, M. Varela, I. C. Tung, M. J. Bedzyk, S. G. Altendorf, F. Strigari, B. Dabrowski, L. H. Tjeng, P. J. Ryan, and J. W. Freeland, Phys. Rev. Lett. **107**, 116805 (2011).

[5] D. Fuchs, C. Pinta, T. Schwarz, P. Schweiss, P. Nagel, S. Schuppler, R. Schneider, M. Merz, G. Roth, and H. v. Löhneysen, Phys. Rev. B **75**, 144402 (2007).

[6] D. Fuchs, E. Arac, C. Pinta, S. Schuppler, R. Schneider, and H. v. Löhneysen, Phys. Rev. B **77**, 014434 (2008).

[7] J. W. Freeland, J. X. Ma, and J. Shi, Appl. Phys. Lett. **93**, 212501 (2008).

[8] A. Herklotz, A. D. Rata, L. Schultz, and K. Dörr, Phys. Rev. B **79**, 092409 (2009).

[9]S. Park, P. Ryan, E. Karapetrova, J. W. Kim, J. X. Ma, J. Shi, J. W. Freeland, and W. Wu, Appl. Phys. Lett. **95**, 072508 (2009).
[10]A. Posadas, M. Berg, H. Seo, A. de Lozanne, A. A. Demkov, D. J. Smith, A. P. Kirk, D. Zhernokletov, and R. M. Wallace, Appl. Phys. Lett. **98**, 053104 (2011).
[11]V. Mehta, M. Liberati, F. J. Wong, R. V. Chopdekar, E. Arenholz, and Y. Suzuki, J. Appl. Phys. **105**, 07E503 (2009).
[12]V. Mehta and Y. Suzuki, J. Appl. Phys. **109**, 07D717 (2011).
[13]M. Merz, P. Nagel, C. Pinta, A. Samartsev, H. v. Löhneysen, M. Wissinger, S. Uebe, A. Assmann, D. Fuchs, and S. Schuppler, Phys. Rev. B **82**, 174416 (2010).
[14]G. E. Sterbinsky, P. J. Ryan, J.-W. Kim, E. Karapetrova, J. X. Ma, J. Shi, and J. C. Woicik, Phys. Rev. B **85**, 020403(R) (2012).
[15]M. A. Senaris-Rodriguez and J. B. Goodenough, J. Solid State Chem. **116**, 224 (1995).
[16]S. Maekawa, T. Tohyama, S. E. Barnes, S. Ishihara, W. Koshibae, and G. Khaliullin, *Physics of Transition Metal Oxides* (Springer-Verlag, Berlin, Germany, 2004).
[17]P. M. Raccah and J. B. Goodenough, Phys. Rev. **155**, 932 (1967).
[18]A. Podlesnyak, S. Streule, J. Mesot, M. Medarde, E. Pomjakushina, K. Conder, A. Tanaka, M. W. Haverkort, and D. I. Khomskii, Phys. Rev. Lett. **97**, 247208 (2006).
[19]M. A. Korotin, S. Yu. Ezhov, I. V. Solovyev, V. I. Anisimov, D. I. Khomskii, and G. A. Sawatzky, Phys. Rev. B **54**, 5309 (1996).
[20]P. G. Radaelli and S. W. Cheong, Phys. Rev. B **66**, 094408 (2002).
[21]M. Zhuang, W. Zhang, and N. Ming, Phys. Rev. B **57**, 10705 (1998).
[22]M. W. Haverkort, Z. Hu, J. C. Cezar, T. Burnus, H. Hartmann, M. Reuther, C. Zobel, T. Lorenz, A. Tanaka, N. B. Brookes, H. H. Hsieh, H.-J. Lin, C. T. Chen, and L. H. Tjeng, Phys. Rev. Lett. **97**, 176405 (2006).
[23]K. Knížek, Z. Jirák, J. Hejtmánek, P. Novák, and W. Ku, Phys. Rev. B **79**, 014430 (2009).
[24]J. Kuneš and V. Křápek, Phys. Rev. Lett. **106**, 256401 (2011).
[25]H. Hsu, P. Blaha, R. M. Wentzcovitch, and C. Leighton, Phys. Rev. B **82**, 100406(R) (2010).
[26]K. Gupta and P. Mahadevan, Phys. Rev. B **79**, 020406 (2009).
[27]J. M. Rondinelli and N. A. Spaldin, Phys. Rev. B **79**, 054409 (2009).
[28]H. Hsu, P. Blaha, and R. M. Wentzcovitch, Phys. Rev. B **85**, 140404(R) (2012).
[29]J. Lee, N. Sai, and A. A. Demkov, Phys. Rev. B **82**, 235305 (2010).
[30]G. Fischer, M. Däne, A. Ernst, P. Bruno, M. Lüders, Z. Szotek, W. Temmerman, and W. Hergert, Phys. Rev. B **80**, 014408 (2009).
[31]G. Kresse and J. Furthmüller, Phys. Rev. B **54**, 11169 (1996).
[32]P. E. Blöchl, Phys. Rev. B **50**, 17953 (1994); G. Kresse and D. Joubert, *ibid.* **59**, 1758 (1999).
[33]S. L. Dudarev, G. A. Botton, S. Y. Savrasov, C. J. Humphreys, and A. P. Sutton, Phys. Rev. B **57**, 1505 (1998).
[34]A. I. Liechtenstein, V. I. Anisimov, and J. Zaanen, Phys. Rev. B **52**, R5467 (1995).
[35]J. P. Perdew and A. Zunger, Phys. Rev. B **23**, 5048 (1981).
[36]F. M. F. de Groot, J. C. Fuggle, B. T. Thole, and G. A. Sawatzky, Phys. Rev. B **42**, 5459 (1990).
[37]M. Abbate, J. C. Fuggle, A. Fujimori, L. H. Tjeng, C. T. Chen, R. Potze, G. A. Sawatzky, H. Eisaki, and S. Uchida, Phys. Rev. B **47**, 16124 (1993).
[38]M. Abbate, R. Potze, G. A. Sawatzky, and A. Fujimori, Phys. Rev. B **49**, 7210 (1994).
[39]T. Saitoh, T. Mizokawa, A. Fujimori, M. Abbate, Y. Takeda, and M. Takano, Phys. Rev. B **55**, 4257 (1997).
[40]A. Chainani, M. Mathew, and D. D. Sarma, Phys. Rev. B **46**, 9976 (1992).
[41]P. G. Radaelli and S. W. Cheong, Phys. Rev. B **66**, 094408 (2002).
[42]A. M. Glazer, Acta Cryst. B **28**, 3384 (1972).
[43]P. M. Woodward, Acta Cryst. B **53**, 32 (1997); **53**, 44 (1997).
[44]H. J. Monkhorst and J. D. Pack, Phys. Rev. B **13**, 5188 (1976).
[45]J. B. Goodenough, Phys. Rev. **100**, 564 (1955); J. Phys. Chem. Solid. **6**, 287 (1958); J. Kanamori, *ibid.* **10**, 87 (1959); P. W. Anderson, Solid State Phys. **14**, 99 (1963).
[46]J.-S. Zhou, J.-Q. Yan, and J. B. Goodenough, Phys. Rev. B **71**, 220103(R) (2005).
[47]S. J. May, J.-W. Kim, J. M. Rondinelli, E. Karapetrova, N. A. Spaldin, A. Bhattacharya, and P. J. Ryan, Phys. Rev. B **82**, 014110 (2010).
[48]T. Vogt, J. A. Hriljac, N. C. Hyatt, and P. Woodward, Phys. Rev. B **67**, 140401(R) (2003).
[49]J.-S. Zhou, J.-Q. Yan, and J. B. Goodenough, Phys. Rev. B **71**, 220103(R) (2005).
[50]The bulk modulus of LCO with 0%, 25%, 50%, and 100% concentrations of HS Co^{3+} is calculated to be 203, 186, 181, and 176 GPa, respectively, showing significant softening as the concentration of HS Co^{3+} increases.
[51]The ionic radius of HS Co^{3+} is calculated to be larger than that of LS Co^{3+} by 0.05 Å, which is in good agreement with the experimental values of $r_{LS} = 0.545$ Å and $r_{HS} = 0.61$ Å.
[52]W. A. Harrison, *Electronic Structure and the Properties of Solids* (Dover, Mineola, NY, 1989).
[53]A. J. Millis, Phys. Rev. B **55**, 6405 (1997).
[54]D. I. Khomskii and G. A. Sawatzky, Solid State Comm. **102**, 87 (1997).
[55]To ensure that the FM coupling is robust in a reasonable range of U_{eff}, we tested three U_{eff} values of 3.0, 3.5, and 4.0 eV, yielding $J_{1,out}$ coupling strengths of 3.0, 2.8 and 2.6 meV/pair, respectively.
[56]C. Ederer, C. Lin, and A. J. Millis, Phys. Rev. B **76**, 155105 (2007).
[57]D. Hobbs, G. Kresse, and J. Hafner, Phys. Rev. B **62**, 11556 (2000).